Redox Function of Tetrahydrobiopterin and Effect of L-Arginine on Oxygen Binding in Endothelial Nitric Oxide Synthase†

Vladimir Berka, Hui-Chun Yeh, De Gao, Farheen Kiran, and Ah-Lim Tsai*

Division of Hematology, Department of Internal Medicine, University of Texas Health Science Center, Houston, Texas 77030

Received May 13, 2004; Revised Manuscript Received August 11, 2004

ABSTRACT: Tetrahydrobiopterin (BH_4), not dihydrobiopterin or biopterin, is a critical element required for NO formation by nitric oxide synthase (NOS). To elucidate how BH_4 affects eNOS activity, we have investigated BH_4 redox functions in the endothelial NOS (eNOS). Redox-state changes of BH_4 in eNOS were examined by chemical quench/HPLC analysis during the autoinactivation of eNOS using oxyhemoglobin oxidation assay for NO formation at room temperature. Loss of NO formation activity linearly correlated with BH_4 oxidation, and was recovered by overnight incubation with fresh BH_4. Thus, thiol reagents commonly added to NOS enzyme preparations, such as dithiothreitol and β-mercaptoethanol, probably preserve enzyme activity by preventing BH_4 oxidation. It has been shown that conversion of L-arginine to *N*-hydroxy-L-arginine in the first step of NOS catalysis requires two reducing equivalents. The first electron that reduces ferric to the ferrous heme is derived from flavin oxidation. The issue of whether BH_4 supplies the second reducing equivalent in the monooxygenation of eNOS was investigated by rapid-scan stopped-flow and rapid-freeze-quench EPR kinetic measurements. In the presence of L-arginine, oxygen binding kinetics to ferrous eNOS or to the ferrous eNOS oxygenase domain ($eNOS_{ox}$) followed a sequential mechanism: $Fe(II) \leftrightarrow Fe^{II}O_2 \rightarrow Fe(III) + O_2^-$. Without L-arginine, little accumulation of the $Fe^{II}O_2$ intermediate occurred and essentially a direct optical transition from the Fe(II) form to the Fe(III) form was observed. Stabilization of the $Fe^{II}O_2$ intermediate by L-arginine has been established convincingly. On the other hand, BH_4 did not have significant effects on the oxygen binding and decay of the oxyferrous intermediate of the eNOS or eNOS oxygenase domain. Rapid-freeze-quench EPR kinetic measurements in the presence of L-arginine showed a direct correlation between BH_4 radical formation and decay of the $Fe^{II}O_2$ intermediate, indicating that BH_4 indeed supplies the second electron for L-arginine monooxygenation in eNOS.

Nitric oxide synthase (NOS)[1] is a self-sufficient P450-like hemoprotein catalyzing conversion of L-arginine (L-Arg) to nitric oxide (NO) and L-citrulline via a stable intermediate, L-*N*-hydroxyarginine (L-NHA) (*1*−*4*). There are three known isozymes of NOS; all have a common bidomain structure, with the reductase domain containing FAD, FMN cofactors, and a NADPH binding site, and the oxygenase domain containing the heme center, tetrahydrobiopterin (BH_4), and a binding site for L-Arg (*1*−*4*). The heme and flavin cofactor contents in NOS have been reliably determined to be close to stoichiometric (*1*−*4*). NOS is the only known P450-like enzyme that requires BH_4 for activity (*7*). Purified NOS shows a BH_4 content much lower than one per subunit and has to be reconstituted to recover the full activity of NO formation (*5*−*7*). The BH_4 content in purified NOS is variable, but correlation between the replenished BH_4 level and NO formation activity indicates maximal activity at a 1:1 stoichiometric ratio (*8*, *9*). Characterization of the BH_4 content is further complicated by autoxidation of BH_4 (*10*, *11*). It has been a common practice to add excess BH_4 and reductant, such as dithiothreitol (DTT), to NOS preparations to guarantee sufficient BH_4 (*12*, *13*). The ability of BH_4 to serve both as specifically bound cofactor and as nonspecific competitive ligand can complicate data interpretation for ligand binding kinetics (*14*), so more attention needs to be paid to this issue of excess BH_4. It is also unclear whether DTT or other reductants are adequate to protect against BH_4 oxidation to 7,8-dihydrobiopterin (BH_2) or even biopterin (B). To address these issues, we have determined the redox-state changes of BH_4 bound to eNOS for comparison with the NO formation activity.

The heme and flavin cofactors have well-identified functions in NOS oxidation/reduction processes (*1*−*4*). The main functional roles attributed to BH_4 include dimerization of iNOS, enhancement of L-Arg binding, facilitation of heme reduction, and heme spin-state transition (*7*, *15*). All these functions can be accomplished by BH_2 (*15*). However, BH_2

† This work was supported by U.S. Public Health Service Grant GM56818 (A.-L.T.).

* To whom correspondence should be addressed. Phone: (713) 500-6771. Fax: (713) 500-6810. E-mail: Ah-Lim.Tsai@uth.tmc.edu.

[1] Abbreviations: NO, nitric oxide; NOS, nitric oxide synthase; nNOS, neuronal NOS; iNOS, inducible NOS; eNOS, endothelial NOS; $eNOS_{ox}$, eNOS oxygenase domain; BH_4, (6*R*)-5,6,7,8-tetrahydro-L-biopterin; BH_4(+) eNOS, BH_4-reconstituted eNOS; BH_4(−) eNOS, BH_4-deficient eNOS; CaM, calmodulin; L-NHA, L-*N*-hydroxyarginine; BH_2, 7,8-dihydrobiopterin; B, biopterin; DTT, dithiothreitol; DTE, 1,4-dithioerythritol; DETAPAC, diethylenetriaminepentaacetic acid; Sf9 cells, *Spodoptera frugiperda* cells; Fe(III), ferric heme; Fe(II), ferrous heme; $Fe(II)O_2$, oxyferrous heme; HbO_2, oxyhemoglobin; RFQ, rapid freeze quench; EPR, electron paramagnetic resonance; rR, resonance Raman; FTIR, Fourier transform infrared.

10.1021/bi049026j CCC: $27.50
Published on Web 09/25/2004

does not support NO biosynthesis, demonstrating that the biopterin redox state is crucial for NOS catalytic activity. On paper, it is possible to devise reaction mechanisms without BH_4 participation based on a conventional P450 monooxygenase reaction that accounts for conversion from L-Arg to L-NHA and then to NO and L-citrulline (*16*, *17*). In reality, however, BH_4 is absolutely essential for both L-NHA and NO formation (*8*, *9*).

Oxygen binding to the ferrous heme, which has a neutral porphyrin core, is essential for both steps of NOS catalysis. Studies by rapid-scan diode array measurements demonstrated that oxygen binding to ferrous NOS or NOS_{ox} follows a sequential mechanism: $Fe(II) \rightarrow Fe^{II}O_2 \rightarrow Fe(III)$ (*18*, *19*). Regulation of oxygen binding by L-arginine and/or BH_4 was anticipated due to the intimate relationship between the heme and binding sites for L-arginine and BH_4 (*20*, *21*). Although L-arginine was reported to show little effect on oxygen binding kinetics in nNOS and eNOS (*18*, *19*), other studies showed a wide range of effects of L-arginine on the binding of other gaseous ligands such as CO and NO (*14*, *22*−*27*). In addition, the large shift of the absorption peak position of oxyferrous heme complex in the presence and absence of substrate (*18*, *28*−*33*) suggested that L-arginine might affect the oxygen binding mechanism. In this study, we found that L-Arg has a substantial effect on oxygen binding, indicating that substrate binding modulates the oxygen binding mechanism.

On the other hand, BH_4 was reported to enhance the degradation of the oxyferrous complex in nNOS (*18*). Whether a similar BH_4 effect on oxyferrous decay kinetics is present in the eNOS isozyme was determined by an oxygen binding kinetic measurement in this study.

The source of the second electron that is needed for peroxyferric heme complex formation during conversion from L-Arg to L-NHA has been enigmatic. The possibility that BH_4 supplies the second reducing equivalent in the monooxygenation was investigated by rapid-scan stopped-flow and rapid-freeze-quench (RFQ) EPR kinetic measurements (*34*−*37*). A BH_4-derived radical was observed when ferrous $iNOS_{ox}$ was reacted with oxygen in the presence of L-Arg (*34*−*37*). EPR line shape changes were observed with $[^{15}N]BH_4$ and with D_2O buffer exchange, confirming that the radical was located on the biopterin and interacted with exchangeable proton(s) (*34*, *36*). Formation of this BH_4-derived radical species was fast, and it accumulated to significant levels. Recently, we were able to trap the BH_4 radical in $eNOS_{ox}$ that had only stoichiometric, specifically bound BH_4 (*38*). A kinetic correlation was observed between $Fe^{II}O_2$ decay and BH_4 radical formation in $iNOS_{ox}$, supporting a functional role for BH_4 as the donor of the second electron in the monooxygenase reaction (*35*). The BH_4-derived radical was also observed in $iNOS_{ox}$ when L-NHA was substituted for L-Arg (*34*, *39*). The kinetic relationship between BH_4 radical formation and eNOS heme redox changes in the presence of oxygen and L-Arg is examined in this study. We confirmed the good kinetic correlation between decay of oxyferrous heme and formation of BH_4 radical.

EXPERIMENTAL PROCEDURES

Materials. BH_4, BH_2, and B were obtained from Schircks Laboratories (Jona, Switzerland). All other chemicals were obtained from Sigma. Sf9 cells were purchased from Pharmingen.

Expression and Purification of the Human eNOS and eNOS Oxygenase Domain ($eNOS_{ox}$). Recombinant human eNOS was prepared using a baculovirus expression system as previously described (*40*). Bovine eNOS and $eNOS_{ox}$, which are BH_4-deficient, were expressed in *Escherichia coli* and purified as described by Martásek et al. (*41*). Human eNOS was expressed in yeast using a *Pichia* expression kit (Invitrogen, CA) similar to that previously described (*38*). Full-length human eNOS expressed in yeast had a very low biopterin content (analysis method described below). The biopterin content of the purified $eNOS_{ox}$ from yeast expression was less than 0.2 per subunit, mainly present as BH_2. All eNOS preparations were stored at liquid nitrogen temperature in buffer containing 50 mM HEPES, pH 7.5, 10% glycerol, and 0.15 M NaCl. BH_4(+) eNOS and BH_4-(+) $eNOS_{ox}$ were prepared by anaerobic incubation of purified proteins with 1 mM BH_4 overnight at 4 °C. Excess BH_4 was removed by gel filtration through a 30 × 1.5 cm column of Bio-Gel P-6DG (Bio-Rad) at 4 °C. Protein fractions were pooled, concentrated by Centriprep 30 (Amicon), and stored at liquid nitrogen temperature in the buffer described above.

Assays of Enzyme Activity. NOS activity was assayed as NO formation using the optical changes of oxyhemoglobin at 401−411 nm (ϵ = 19.7 mM^{-1} cm^{-1}) (*42*). Briefly, 100 nM eNOS was added to 1 mL of 50 mM HEPES buffer, pH 7.5, containing 10 μM HbO_2, 1 mM L-Arg, and 0.1 mM Ca^{2+}, 0.1 mg CaM at 24 °C and 100 μm NADPH to start each assay. Typical specific activities for bovine and human eNOS were 70−120 nmol of NO/min/mg.

Biopterin Determination. The total biopterin content of purified eNOS was measured using the procedure described previously (*43*). Quantitation of individual biopterin redox species in eNOS or $eNOS_{ox}$ was conducted by a combination of chemical quench and HPLC as detailed in the Results. The HPLC system comprised a Waters 510 HPLC pump, a model 680 automated gradient controller, a Rheodyne 7125 injector, a Hewlett-Packard series 1100 photodiode array detector, and Agilant Chemstation software for data collection and analysis.

Stopped-Flow Experiments. Binding and dissociation rate constants, k_{on} and k_{off}, were determined by kinetic measurements on an Applied Photophysics model SX-18MV stopped-flow instrument with a rapid-scan diode array accessory (*14*). For anaerobic experiments, the fluid channels were incubated with a dithionite solution for several hours and then washed with nitrogen-saturated buffer. Reactants were rendered anaerobic by repeated vacuum/Ar cycles in a tonometer. The reaction time courses were analyzed by nonlinear regression to single- or multiple-exponential functions. Estimated k_{on} and k_{off} values were derived from the slope and *y*-intercept, respectively, in plots of k_{obs} versus ligand concentrations.

Biopterin Radical Formation Kinetics in $eNOS_{ox}$. The procedure was essentially the same as that recently described (*38*). Ferrous $eNOS_{ox}$ prepared by anaerobic titration with a minimal amount of dithionite to shift the heme Soret peak to 412 nm, or by photoreduction in the presence of deazaflavin and 1 mM EDTA, was reacted with oxygenated buffer. Samples at different reaction time points were collected for EPR analysis by the rapid-freeze technique

using an Update Instrument (Madison, WI) system 1000 rapid-freeze apparatus placed inside an anaerobic chamber (Coy Laboratory, MI).

Spectrometry. UV−vis spectra were recorded with an HP8453 diode array spectrophotometer with a 1 nm spectral bandwidth. EPR spectra were recorded at liquid helium or liquid nitrogen temperatures on a Bruker EMX spectrometer (*38*). Data analysis were conducted using WinEPR programs furnished with the EMX system. The conditions for liquid nitrogen EPR measurements were microwave power 2 mW, frequency 9.29 GHz, modulation amplitude 2 G, modulation frequency 100 kHz, and time constant 0.33 s. Liquid helium EPR conditions were the same, except with microwave power 1 mW, frequency 9.61 GHz, and modulation amplitude 10 G. The microwave power dependence was analyzed by nonlinear regression to the equation $\log(S/P^{1/2}) = -(b/2)\log(P^{1/2} + P) + (b/2)\log(P^{1/2}) + \log K$, where P is the power, S is the peak to trough amplitude of the EPR signal, $P^{1/2}$ is the power at half-saturation, and b and K are floating parameters (*44*).

Computer Modeling. ProK software (Applied Photophysics) was used to conduct global analysis of diode array stopped-flow data after singular value decomposition (SVD) based on the mechanistic model described later in the text.

RESULTS

Determination of BH_4 Chemical Stability. The effects of pH, reducing agents, and metal chelators on the chemical degradation of BH_4 were first assessed using spectroscopic measurements. The decay rates obtained by exponential fitting to the kinetic data were compared with literature results to select the optimal solvent composition to stabilize BH_4 (data not shown). Most of the tested buffer systems between pH 6.8 and pH 8.2 proved ineffective in decreasing BH_4 decay (*45*). Lowering pH alone was not sufficient to give maximal protection against BH_4 decay, as BH_4 in pH 0.3 buffer containing ascorbic acid, perchloric acid, EDTA, and $Na_2S_2O_3$ still decayed at $\sim$0.0023 min^{-1} (*46*). BH_4 exhibited a decay rate as slow as 0.0005 min^{-1} in very acidic perchloric acid plus either ascorbic acid or DTE (*47*), but an even slower BH_4 decay, $<$0.0004 min^{-1}, was observed in cerebrospinal fluid at neutral pH containing DTE and DETAPAC (*48*). In our hands, BH_4 at neutral pH degraded at 0.017 min^{-1}, with DTT decreasing the decay rate about 4-fold. Lowering the pH from 7.0 to 3.0 led to 3-fold slower degradation; further addition of DTT did not reduce the rate significantly. As the HPLC column matrix used for subsequent resolution of biopterins becomes unstable at pH lower than 2.0, we decided to use pH 3 quenching solvent as a compromise. We finally chose a quench solution containing 6.5 mM dibasic sodium phosphate, 6 mM citric acid, 5 mM DTE, 2.5 mM DETAPAC, 3 mM 1-octanesulfonic acid, and 10% methanol (extraction buffer). This quenching solution gave a 0.001 min^{-1} decay rate constant for BH_4 and was also suitable for the HPLC running buffer.

To test the extraction/chromatography procedure, we first added equal amounts of BH_4, BH_2, and B to the extraction buffer. This mixture was vortexed for 1 min, injected into a 250 × 4.6 mm Phenomenex Luna 5 μm C-18 HPLC column, and eluted with the extraction buffer at 1 mL min^{-1}; the eluate was monitored at A_{266nm} using a Hewlett-Packard series 1100 photodiode array detector. A typical chromatogram is shown in Figure 1 (trace a) with B, BH_2, and BH_4 eluting at 6.2, 8.3, and 11 min, respectively. The amount of each biopterin redox species was quantified by integration of the corresponding peak, with reference to standard curves for each biopterin species. These standard curves were linear from 10 to 1000 pmol (data not shown). The eluted biopterins retained the initial 1:1:1 stoichiometry, indicating that there were no changes in the redox state of biopterins during extraction and HPLC.

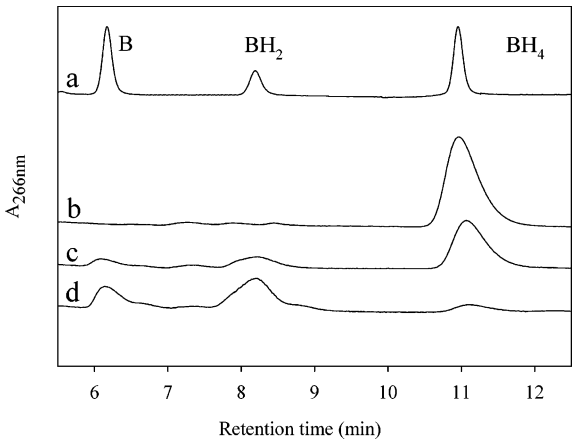

FIGURE 1: HPLC of biopterins. Chromatograms are shown for an extracted mixture of BH_4, BH_2, and B standards (100 pmol each) (a) and biopterins extracted from BH_4(+) eNOS at 0 (b), 3.5 (c), or 6.0 (d) h of incubation at 24 °C. Details are described in the Results.

Relationship between BH_4 Oxidation and Loss of NO Formation Activity in eNOS. A sample of eNOS purified from Sf9 cells and reconstituted with fresh BH_4 as previously described (*14*) was incubated at room temperature in 50 mM HEPES, pH 7.4, containing 0.1 M NaCl and 10% glycerol. Aliquots were removed at 0, 3.5, and 6 h and chemically quenched in the BH_4 extraction buffer described above. Denatured protein was removed by centrifugation (5 min at 12000 rpm), and the supernatant was analyzed by HPLC (Figure 1, traces b−d). Initially, all biopterin in the enzyme was present as BH_4, but substantial conversion from BH_4 to BH_2 and B occurred during incubation at room temperature (Figure 1). To assess the effect of BH_4 oxidation on eNOS activity, we monitored the NO formation activity and biopterin redox state of BH_4(+) eNOS during enzyme incubation at either 4 or 24 °C (Figure 2). BH_4(+) eNOS incubated on ice led to little activity loss or BH_4 oxidation after 6 h (Figure 2A). In contrast, BH_4(+) eNOS incubated at 24 °C showed a time-dependent decay of NO formation activity as well as a conversion from BH_4 to BH_2 and B (Figure 2A); the rate constant for decay of BH_4 or NO formation activity was 0.006 min^{-1}. This decay rate constant is substantially smaller than for decay of free BH_4 at neutral pH, indicating that BH_4 was protected by binding to eNOS. To determine if BH_4 oxidation was the cause of enzyme activity loss, we incubated an eNOS sample for 24 h at room temperature, assayed the NO formation activity and BH_4 redox state, and then reconstituted with fresh BH_4 (Figure 2B). There was about 5% residual enzyme activity after 24 h of incubation of BH_4(+) eNOS at 24 °C (Figure 2B, point 2). Addition of a stoichiometric amount of BH_4 immediately increased the enzymatic activity to $\sim$25% of that of the zero time BH_4(+) eNOS control (point 3). Further anaerobic

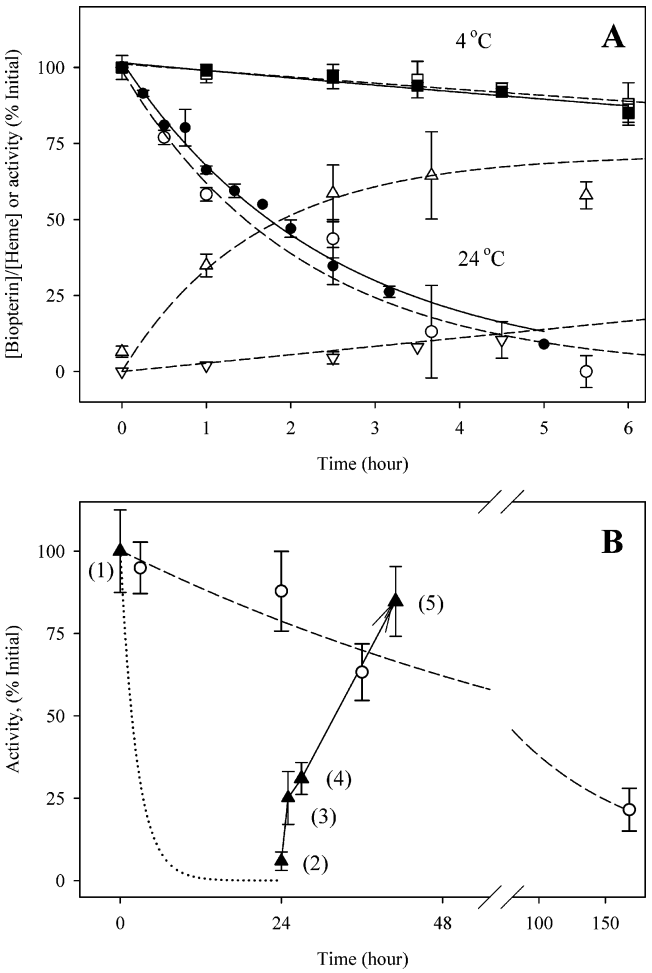

FIGURE 2: Decay of eNOS activity and BH_4 and the reversible recovery of NO formation activity in eNOS. **(A)** Purified $BH_4(+)$ eNOS, 30 μM, was incubated at 24 °C, and aliquots were taken at the indicated times for assay of BH_4 (open circles), BH_2 (triangles), B (inverted triangles) contents and NO formation activity (solid circles). A separate $BH_4(+)$ eNOS sample was incubated at 4 °C for the indicated times and assayed for BH_4 content (open squares) and NO formation activity (solid squares). Data shown are obtained from two experiments with error bars indicating 3−6 repeats. (B) The activity of purified $BH_4(+)$ eNOS was measured before and after incubation at ambient temperature for 24 h (first two solid triangles). Data point 3 indicates the activity immediately after addition of an equimolar amount of fresh BH_4. Recovery of activity by anaerobic incubation with an excess of BH_4 for ∼2 and ∼16 h was measured after gel filtration (points 4 and 5, respectively). The error bars are the standard deviations of three duplicate assays at each time point. The dotted line is the theoretical decay curve at 0.006 min^{-1} calculated from (A), and the arrow indicates the recovery of activity. A 100 nM concentration of $BH_4(-)$ eNOS was also monitored for its NO formation activity loss at 24 °C (open circles). All data in (A) and (B) were normalized to initial activity. The lines are the fits to a one-exponential function.

incubation with excess BH_4 led to gradual recovery of activity from 30% (after 2 h) (point 4) to 85% (after 16 h) (point 5) when excess BH_4 was removed by gel filtration before activity analysis. The average activity recovered from $BH_4(+)$ eNOS after 16 h of incubation was 84.7 ± 10.6% ($n = 6$) of the initial value. In a control experiment, $BH_4(-)$ eNOS was incubated at room temperature and NO formation activity was analyzed in the presence of fresh BH_4 (Figure 2B). The activity loss in this case was very slow (0.007 h^{-1}), about 40 times slower than for $BH_4(+)$ eNOS. About 70% of the activity of $BH_4(-)$ eNOS remained at 40 h, the time corresponding to the total incubation used for the $BH_4(+)$ samples (24 h of aerobic incubation, 16 h of anaerobic incubation with fresh BH_4). Thus, reconstitution with fresh BH_4 restored essentially all activity in oxidized eNOS, showing that the loss of activity upon BH_4 oxidation was fully reversible.

Effect of L-*Arg on Oxygen Binding to eNOS and* $eNOS_{ox}$. Since BH_4 radical formation has been used as an activity index of $eNOS_{ox}$ and BH_4 redox function (*38*), and reaction of ferrous $eNOS_{ox}$ with oxygen triggers BH_4 radical production if L-Arg is present (*34*−*38*), it was thus important to examine the effect of L-Arg on oxygen binding to the ferrous heme in eNOS/$eNOS_{ox}$. $BH_4(+)$ $eNOS_{ox}$ was converted to the ferrous form by careful anaerobic titration with dithionite to avoid excess reductant. The ferrous enzyme was then mixed at 4 °C with buffer containing 150 μM oxygen and the reaction monitored by rapid-scan diode array stopped-flow measurements. In the presence of L-Arg (250 μM), there were two stages of spectral changes over the first few seconds (Figure 3A). The first stage lasted ∼100 ms and involved a Soret band shift from 412 nm (ferrous form) to 427 nm, with an isosbestic point at 425 nm. The second stage lasted for several seconds and included a shift of the Soret peak from 427 to 397 nm (ferric form), with an isosbestic point at 419 nm. Similar results were obtained with full-length eNOS. Overall, the spectral changes indicate a reaction sequence of Fe(II) ↔ $Fe^{II}O_2$ → Fe(III), with the $Fe^{II}O_2$ intermediate having a Soret peak at 427 nm. In contrast, parallel kinetic measurements in the absence of L-Arg showed much smaller changes in the first 15 ms period, and the dominant changes were at the second-stage reaction. There was little indication of initial accumulation of the 427 nm intermediate, but rather a quick transition from the 412 nm species (ferrous form) through the 418 nm intermediate (mixture of ferrous, ferric, and oxyferrous species) to the 404 nm species (mixture of high- and low-spin ferric forms) (Figure 3B). Single-wavelength kinetic data at 400 and 428 nm retrieved from the rapid-scan kinetic data also revealed the much lower accumulation of the $Fe^{II}O_2$ intermediate in the reaction without L-Arg (Figure 3, Insets). Similar results were obtained for $BH_4(-)$ eNOS or $BH_4(-)$ $eNOS_{ox}$, indicating a minimal effect from BH_4 on the oxygen binding mechanism.

As $Fe^{II}O_2$ was transiently formed during ferrous heme interaction with O_2 in the presence of L-Arg, it was important to characterize the binding and decay rate constants to define the reaction mechanism. Binding of oxygen to Fe(II) $eNOS_{ox}$ was relatively fast, so we conducted the binding kinetic measurements at 4 °C to allow measurements of the rates over a wider oxygen concentration range. Single-wavelength stopped-flow observations were made at 400, 408, and 428 nm and yield similar information for kinetic parameters. The rate constants determined under pseudo-first-order conditions are summarized in Table 1. In the presence of L-Arg, the observed absorbance change at 400 nm upon oxygen binding was large, and the rate could be precisely defined (indicated by the small error bars in Figure 4A). The observed rate was linear from 10 to 150 μM oxygen. Oxygen association with the Fe(II) heme in the absence of L-Arg was also linearly dependent on [O_2] and was ∼7−8-fold faster than when L-Arg was present. Data fluctuations were much larger in the absence of L-Arg, as much smaller absorbance changes were observed (Figure 4). This fluctuation cannot be

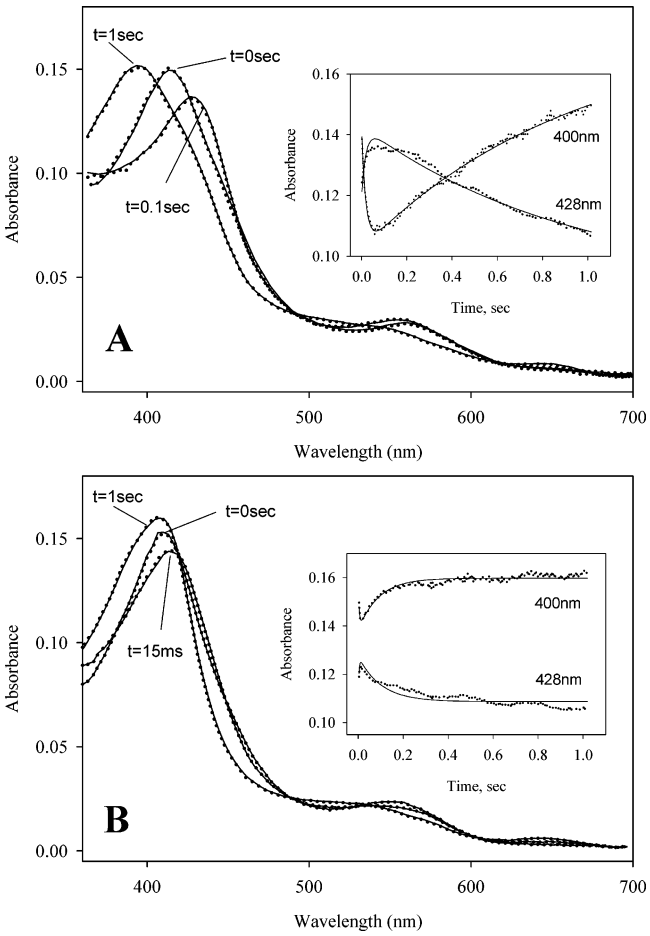

FIGURE 3: Effects of L-Arg on oxygen binding to ferrous eNOSox. An anaerobic solution of 3−5 μM ferrous $BH_4(+)$ $eNOS_{ox}$ either with (A) or without (B) 250 μM L-Arg was mixed with an air-saturated buffer solution at 4 °C, and the spectra were collected at 2.5 ms intervals using a rapid-scan diode array detector. Spectra acquired at 0 and 1 s for initial ferrous heme and final ferric heme as well as the spectra exhibiting the largest red shift for $Fe^{II}O_2$ formation are shown. The insets in (A) and (B) show kinetic data and the fit at 400 and 428 nm retrieved from the rapid-scan data and global analysis. Optimal values used for global analyses were $k_1 = 51\ s^{-1}$, $k_{-1} = 2.5\ s^{-1}$, and $k_2 = 1.1\ s^{-1}$ in (A) and $k_1 = 250\ s^{-1}$, $k_{-1} = 59\ s^{-1}$, and $k_2 = 12\ s^{-1}$ in (B), with k_1 in units of the pseudo-first-order rate constant. In both the main figure and the insets, dots are the original optical data and lines are the global fits to the mechanistic model represented by eq 4.

improved by collecting data at 408 or 412 nm (data not shown). The dissociation rate constant (k_{-1}) estimated from the *y*-intercept decreased from 50−60 to ∼2−6 s^{-1}, in the presence of L-Arg (Figure 4A and Table 1).

BH_4 had little effect on the k_{on} and k_{off} of oxygen binding to $eNOS_{ox}$: $1.47 \times 10^6\ M^{-1}\ s^{-1}$ and $59.9\ s^{-1}$ in the absence of L-arginine and $0.4 \times 10^6\ M^{-1}\ s^{-1}$ and $5.5\ s^{-1}$ in the presence of L-arginine, respectively (Figure 4B). The decay kinetics of $Fe^{II}O_2$ were quantitated as the down phase in A_{400}. In the presence of L-arginine, there is only one phase with the rate constant at 0.25 or 1.4 s^{-1}, $BH_4(-)$ or $BH_4(+)$, respectively. In the absence of L-arginine, biphasic decay was observed with rate constants in the range of 10−40 (fast) and 0.45 (slow) s^{-1} and 5−20 (fast) and 1.1 (slow) s^{-1} in the absence and presence of BH_4, respectively.

To confirm the effect of L-Arg on the oxygen binding kinetics in the full-length enzyme, experiments similar to those in Figure 4 were performed using $BH_4(-)$ eNOS. The results, shown in Table 1, indicated that L-Arg decreased the oxygen binding rate constant from 1.8×10^6 to $3.2 \times 10^5\ M^{-1}\ s^{-1}$ and k_{off} from 48 to $7.2\ s^{-1}$ in $BH_4(-)$ eNOS, similar to those found for $BH_4(-)$ $eNOS_{ox}$. BH_4 had only minor effects on O_2 binding to eNOS. In the absence of L-Arg, the on rate constant was $1.4 \times 10^6\ M^{-1}\ s^{-1}$ and the off rate constant was $60\ s^{-1}$. In the presence of L-Arg, the values for k_{on} and k_{off} were $3.9 \times 10^5\ M^{-1}\ s^{-1}$ and $9.2\ s^{-1}$, respectively. The $Fe^{II}O_2$ decay kinetics for the full-length eNOS sample were biphasic in the presence or absence of L-arginine with 30−50% absorbance contribution from the fast phase (see Table 1). The samples without L-arginine showed much faster rates for both phases, 12 vs $0.7\ s^{-1}$ in the fast phase and 1.2 vs $0.15\ s^{-1}$ in the slow phase, respectively (Table 1). The same trend was found for experiments using $BH_4(+)$ eNOS: 5−30 vs $3.0\ s^{-1}$ and 1.0 vs $0.25\ s^{-1}$ with and without L-arginine, respectively. Overall, L-Arg binding significantly decreased both k_{on} and k_{off} for oxygen binding and also decreased the overall decay rate of the $Fe^{II}O_2$ complex (Table 1). BH_4 appears to have a minimal influence on the oxygen binding mechanism.

Kinetics of the BH_4 Radical and $Fe^{II}O_2$ Intermediate. BH_4 radical formation during the reaction between ferrous $eNOS_{ox}$ and oxygenated buffer (130 μM oxygen) at 24 °C was monitored by rapid-freeze-quench EPR spectrometry. There was no BH_4 radical formation in the absence of L-Arg, so all experiments were done in the presence of 0.5 mM L-Arg. A single type of EPR spectrum was observed for samples trapped at all time points (Figure 5), and the spectrum resembled that previously reported for the BH_4 radical (*38*), with a *g* value of 2.0023 and an overall line width of 40 G. The $P^{1/2}$ value was 14 mW at 120 K (Figure 5, inset), close to that previously reported for the BH_4 radical (*38*). To assess the kinetic relationship between heme redox changes and BH_4 radical formation, we did parallel stopped-flow and RFQ experiments using $BH_4(+)$ $eNOS_{ox}$ preparation. The accumulation of $Fe^{II}O_2$, followed at 427 nm, showed an initial fast rise in less than 25 ms, followed by an exponential decay with a rate around $9\ s^{-1}$ (Figure 6A). The freeze-quench samples were analyzed by EPR at 11 K for the $g = 7$ (ferric heme) and $g = 2$ (biopterin radical) signal amplitudes. The same samples were also analyzed at 115 K to quantitate the spin concentration by double integration with reference to a copper standard; the radical signal amplitude measured at 11 K was linearly correlated with the spin concentration (data not shown). The increases in the $g = 7$ and $g = 2$ signals showed similar rates, 9.8 and $11.2\ s^{-1}$, respectively, and paralleled the decreases in $Fe^{II}O_2$ monitored by A_{427} (Figure 6A). Conversion of $eNOS_{ox}$ $Fe^{II}O_2$ to the Fe(III) form thus coincided very well with BH_4 radical formation. BH_4 radical formation was transient, decaying at a rate of about $0.3\ s^{-1}$ (Figure 6B) without obvious accompanying heme optical spectral changes.

DISCUSSION

1. Quantification of All Redox States of Free or eNOS-Bound Biopterin.

a. Function of BH_4. BH_4 was reported to be necessary for iNOS dimerization (*49*, *50*), but recent results indicate this is not true for any NOS isozyme (*51*, *52*). Rather, it appears that heme plays the critical role in eNOS dimerization (*51*,

Table 1: Kinetics of Oxygen Binding at 4 °C

conditions	k_{on} (M^{-1} s^{-1})	k_{off} (s^{-1})	K_d[a] (μM)	decay rate (s^{-1})
$eNOS_{ox}$, $-BH_4$ − L-arg	$(1.95 \pm 0.1) \times 10^6$	54 ± 11	27.7 ± 5.8	10−40,[b] first phase 0.45, second phase
$eNOS_{ox}$, $-BH_4$ + L-arg	$(2.3 \pm 0.3) \times 10^5$	2.25 ± 0.2	9.8 ± 1.6	0.25
$eNOS_{ox}$, $+BH_4$ − L-arg	$(1.47 \pm 0.4) \times 10^6$	59.9 ± 9	40.7 ± 12.6	5−20,[b] first phase 1.1, second phase
$eNOS_{ox}$, $+BH_4$ + L-arg	$(4.0 \pm 2.0) \times 10^5$	5.5 ± 4	13.8 ± 12.2	1.4
eNOS, $-BH_4$ − L-arg	$(1.8 \pm 0.2) \times 10^6$	48 ± 2	26.6 ± 6.2	12, first phase, 50% 1.2, second phase
eNOS, $-BH_4$ + L-arg	$(3.2 \pm 1.4) \times 10^5$	7.2 ± 3.1	22.5 ± 13.8	0.7, first phase, 40% 0.15, second phase
eNOS, $+BH_4$ − L-arg	$(1.4 \pm 0.7) \times 10^6$	60 ± 8	43 ± 22.2	5−30,[b] first phase, 30% 1.0, second phase
eNOS, $+BH_4$ + L-arg	$(3.9 \pm 1.0) \times 10^5$	9.2 ± 5	23.6 ± 14.2	3.0, first phase, 50% 0.25, second phase

[a] Calculated as the ratio k_{off}/k_{on}. [b] Exhibited a saturating oxygen concentration dependence. The reason for this phenomenon is unclear. The percentage of each phase is hard to determine in this case.

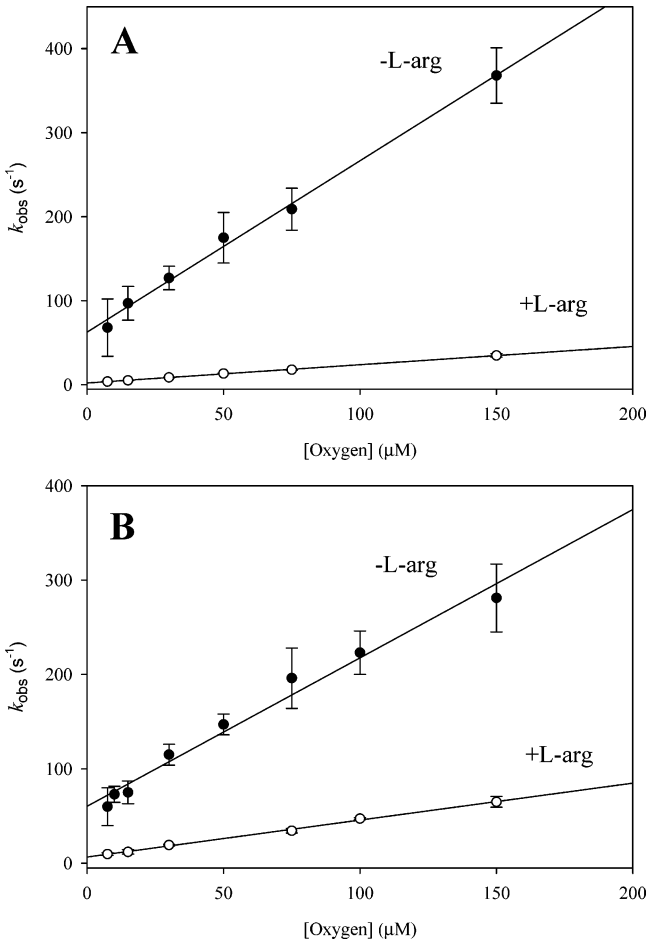

FIGURE 4: Relationship between oxygen concentration and the observed rate for $Fe^{II}O_2$ formation. Ferrous BH_4(−) $eNOS_{ox}$ (5 μM) (A) and BH_4(+) $eNOS_{ox}$ (5 μM) (B) in the presence (open circles) and absence (closed circles) of 250 μM L-Arg were reacted with buffer containing different levels of oxygen at 4 °C, the biphasic kinetic data at 400 nm were fit by a one-exponential function for each phase, and the observed rates were plotted against oxygen concentrations. Bars indicate the standard error means for 3−5 measurements averaged and mostly lie within the circles for +L-Arg.

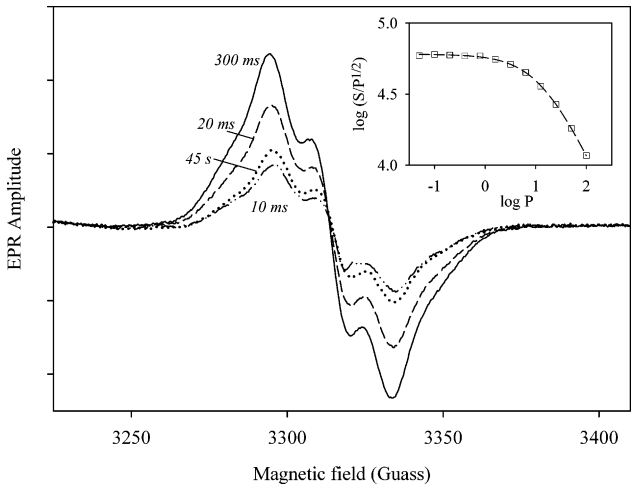

FIGURE 5: Formation of BH_4 radical in $eNOS_{ox}$. $eNOS_{ox}$ (50 μM) containing 0.7 equiv of BH_4/heme in 50 mM HEPES, pH 7.4, with 10% glycerol, 0.1 M NaCl, and 1 mM L-Arg was made anaerobic and stoichiometrically reduced with dithionite. The ferrous $eNOS_{ox}$ was then reacted with an equal volume of oxygenated buffer at 24 °C and quenched into prechilled isopentane. EPR spectra were recorded at 115 K for samples freeze quenched at 10 ms (dashed−dotted−dotted line), 20 ms (dashed line), 300 ms (solid line), 45000 ms (dotted line). The inset shows the microwave power dependence of the BH_4 radical.

53). Crystallographic data show the NOS-like protein from *Staphylococcus aureus* (SA-NOS), which lacks the zinc binding domain and BH_4, is also a dimer, with a K_d value of ~20 nM, similar to that of dimeric $eNOS_{ox}$ (*54*, C. S. Raman, personal communication). A very similar situation was found with another NOS-like protein from *Bacillus subtilis* (*55*). L-Arg and BH_4 mutually enhance their binding in nNOS and eNOS (*52*, *53*, *56*). An extensive H-bonding network connects the structural "triad", heme/BH_4/L-Arg; thus, binding of each component could rigidify the structure of the heme distal pocket (*20*, *21*). Similarly, the heme spin-state shift from low to high spin caused by BH_4 and/or L-arginine may simply be a result of rigidifying the heme pocket and expelling a water molecule from the heme distal site (*9*, *15*). Therefore, the most important function of BH_4 in NOS appears to be a redox participant.

b. New Method for BH_4 Redox-State Analysis. Defining the role of BH_4 in NOS redox reactions obviously requires an effective method to monitor biopterin redox-state changes. Conventional fluorescence methods for quantifying biopterin require conversion of all biopterins to the oxidized form (*43*, *57*, *58*) without distinguishing the individual redox state of

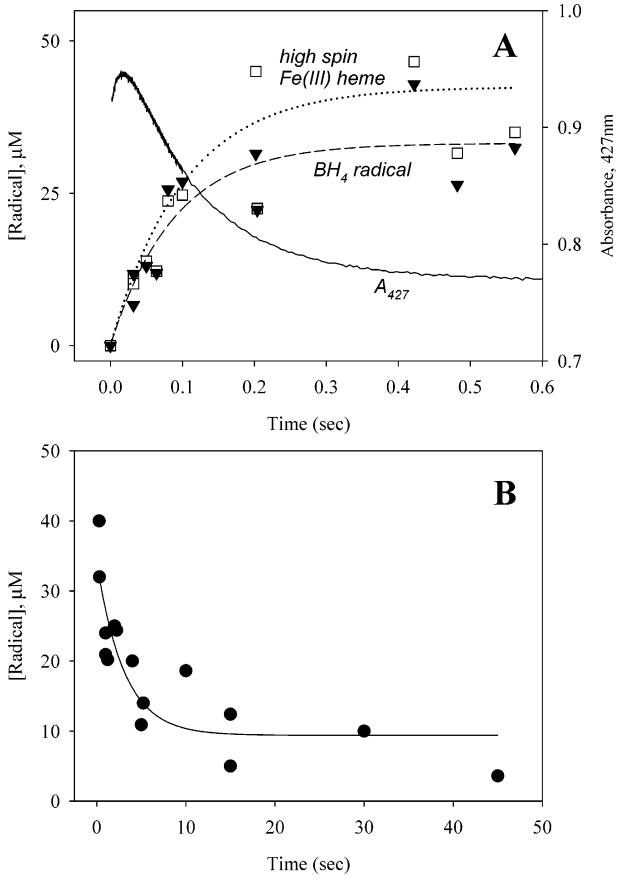

FIGURE 6: Tetrahydrobiopterin radical kinetics during reaction of reduced eNOSox with oxygen in the presence of L-Arg. (A) Samples from the experiment described in Figure 5 were analyzed at 11 K to obtain amplitudes of both the radical signal at $g = 2$ (triangles) and the ferric heme high-spin signal at $g = 7$ (squares). Parallel stopped-flow kinetic data were also acquired by single-wavelength stopped-flow measurements at 427 nm (solid line). Exponential fits to the ferric heme and BH_4 radical signal intensities are shown. (B) Biopterin radical decay kinetics obtained from this same set and one other set of experiments. The solid line represents the exponential fit. The radical level determined either from the $g = 2$ peak-to-trough amplitude in the 4000 G scan EPR at 11 K (shown in the figure) or by double integration of the 200 G scan signal against a copper standard at 115 K gave very similar kinetics.

biopterin. Although the BH_4 level can be determined as the difference in biopterin level measured for the same sample under either acidic or basic oxidation, the relative amounts of BH_2 and B cannot be quantified (*59*). The acidic extraction buffer developed in the present study includes thiol and metal chelator and permits simultaneous quench and stabilization of all three biopterin redox states. The extract can be directly used for HPLC analysis because the same extraction buffer was used as the HPLC running buffer. Results from parallel chemical quench/HPLC analyses of BH_4 content and NO formation activity (Figure 2A) strongly indicate that the loss of activity is due to BH_4 autoxidation. The activity loss was reversible upon anaerobic reconstitution with fresh BH_4 in the absence of thiol or other reductant (Figure 2B). Recovery of activity was time dependent, suggesting that the fresh BH_4 displaces oxidized biopterin from the BH_4 binding site on the protein. This assessment was backed by our HPLC analysis for the biopterin stoichiometry and redox state before and after reactivation. The BH_2 present in the inactivated eNOS sample was later completely replaced by BH_4 in the maximally reactivated eNOS (data not shown).

c. Effects of Thiol Reagents. The protective effects of thiol reagents commonly included during eNOS purification and storage (*12*, *13*, *60*−*62*) are most likely a consequence of preventing BH_4 oxidation. Another proposed protective mechanism of thiol in preventing the oxidation of certain cysteine residue(s) (*12*, *61*, *62*) lacks direct supporting evidence and is much less significant than its role in protecting BH_4 oxidation. As a routine, thiol was excluded from our eNOS purification procedure. DTT was only included to prevent BH_4 oxidation after its reconstitution to eNOS. In one experiment similar to that described in Figure 2B, we included 4 mM DTT in BH_4(−) eNOS and found there is no significant protection for the decay of the NOS activity by DTT (data not shown). Thus, the slow decay of the BH_4(−) eNOS probably is not related to oxidation of specific cysteine thiol(s). It will be interesting to see if a similar behavior of bound BH_4 is found for the other NOS isoforms.

d. BH_4 Decay in Free and eNOS-Bound Forms. The oxidation rate of eNOS-bound BH_4 was substantially slower than that of free BH_4 in solution at physiological pH (Figure 2A), indicating that interactions between the eNOS protein and BH_4 stabilize the cofactor. Autoxidation of free BH_4 is oxygen-dependent (*10*, *11*). The reaction seems to start with direct electron transfer from BH_4 to oxygen to generate superoxide. Subsequent proton capture by superoxide yields BH_3* radical and the hydrogen peroxide radical, HO_2* (eq 1). The N3 proton, pK_a at 10.6, is believed to be the proton transferred to superoxide (*11*). The chain propagation reactions involve hydrogen peroxide formation from BH_4 and HO_2* and BH_3* radical reaction with O_2 to regenerate HO_2* (eqs 2 and 3). Termination likely involves recombination of BH_3* and HO_2* radicals.

$$BH_4 + O_2 \rightarrow BH_3^* + HO_2^* \quad (1)$$

$$BH_4 + HO_2^* \rightarrow BH_3^* + H_2O_2 \quad (2)$$

$$BH_3^* + O_2 \rightarrow BH_2 + HO_2^* \quad (3)$$

Initiation of BH_4 autoxidation is not very fast (0.6 M^{-1} s^{-1} at pH 7 and room temperature), but the chain propagation steps proceed relatively quickly (3.9×10^5 and 3.2×10^3 M^{-1} s^{-1} for reactions 2 and 3, respectively) (*63*). Initial electron loss from BH_4 is greatly decreased at acidic pH, because protonation of N5 (pK_a = 5.6) prevents the lone pair electrons from participating in conjugation of the subsequent cation radical. This mechanism explains the small decay constants found in low-pH media.

Additional factors provide further stabilization for eNOS-bound BH_4. H-bonding between heme propionate with the N3−H, as indicated in $eNOS_{ox}$ crystallographic data (*20*, *21*), would inhibit the deprotonation of the imine. Another mechanism of stabilization at low pH could be protonation of N5 to form BH_5^+. Although there is no direct evidence for this in eNOS, binding of L-Arg, which has a positively charged guanidium group, in the BH_4 site in BH_4(−) $eNOS_{ox}$ implies that a cationic form of tetrahydrobiopterin is likely present in native eNOS (*2*, *20*). In iNOS, Arg375 (Arg365 in eNOS) is H-bonded to N5 of BH_4 via a structured water and could stabilize the cofactor by raising the effective pK_a (*64*).

e. Why Treat BH_4 as a Cofactor? Marletta first demonstrated that BH_4 is necessary for NO formation by macrophages (*6*), but whether BH_4 serves as a bound cofactor or a diffusible ligand of NOS was in doubt because isolated NOS or NOS_{ox} usually contains 0.05−0.5 BH_4 molecule per heme (*5*−*8*). BH_4 reconstitution in parallel with enzyme activity analysis in iNOS and nNOS indicates stoichiometries of 1:1 (BH_4:heme) and 0.7−0.8:1 (BH_4:monomer) (*8*, *9*, *17*). Other BH_4 binding studies indicated heterogeneity of BH_4 binding sites and an ambiguous binding stoichiometry (*65*). For our eNOS/$eNOS_{ox}$ preparation, the highest BH_4 stoichiometry obtained was 0.7−0.8 per monomer after removal of excess BH_4 by gel filtration using a reconstitution procedure similar to that described by Marletta (*14*, *38*). Further addition of exogenous BH_4 in the assay led to another ∼20% increase of NO formation activity, but we have treated BH_4 as a cofactor and always removed excess BH_4. This is because excess BH_4 perturbs other ligand binding interactions with the oxygenase domain by acting as a free ligand, and oxidation of free BH_4 is more rapid than that of bound BH_4, further complicating data interpretation. In addition, BH_4 reacts efficiently with superoxide (10^5 M^{-1} s^{-1} at room temperature) (*63*), and could thus change the NOS product profile, considering the efficient trapping of NO by superoxide to form peroxynitrite. The relationship between inactivation of NOS and BH_4 oxidation had not been examined in such a direct manner as our quantitative chemical quench/HPLC analysis. By scrupulously excluding excess biopterin from the NOS preparation, the present results provide the first direct correlation between loss of NOS activity and oxidation of eNOS-bound BH_4 (Figure 2A).

2. Effects of L-Arg on Oxygen Binding to eNOS. The marginal effect of BH_4 but dramatic effect of L-Arg on oxygen binding to ferrous eNOS/$eNOS_{ox}$ was quite different from earlier reports (*18*, *19*). The contrasting optical spectral changes during oxygen binding to ferrous eNOS in the presence and absence of L-Arg were demonstrated in full-length eNOS and $eNOS_{ox}$ (Figures 3−5) and also in *S. aureus* NOS-like protein (data not shown). The data clearly show that L-Arg stabilizes the oxyferrous intermediate; without L-Arg, little oxyferrous heme intermediate accumulated, and there was essentially a direct optical transition from ferrous eNOS to the ferric form (Figure 3B). The *S. aureus* and *B. subtilis* NOS-like proteins have very high structural homology to $eNOS_{ox}$ but do not bind BH_4 (*54*, *55*, Raman et al., personal communication). Thus, the effect of L-Arg on oxygen binding observed here (Table 1) does not involve BH_4. The simplest scheme for oxygen reaction with ferrous eNOS is thus

$$\mathrm{Fe(II)} + \mathrm{O_2} \underset{k_{-1}}{\overset{k_1}{\leftrightarrow}} \mathrm{Fe^{II}O_2} \xrightarrow{k_2} \mathrm{Fe(III)} + \mathrm{O_2^-} \qquad (4)$$

k_1 and k_{-1} are the on and off rate constants for oxygen binding, and k_2 is the rate constant for oxyferrous conversion to ferric heme and superoxide. Global analyses were performed on rapid scan data based on eq 4. As shown in Figure 3A, the optimal values for the rate constants to fit the data obtained in the presence of L-Arg were $k_1 = 51$ s^{-1}, $k_{-1} = 2.5$ s^{-1}, and $k_2 = 1.1$ s^{-1}. In the absence of L-Arg, the optimal values for the three rate constants were 250, 59, and 12 s^{-1}, respectively (Figure 3B). These values coincide with those determined by single-wavelength stopped-flow kinetic measurements (Figure 4). Therefore, L-Arg addition caused a significant decrease of all three rate constants. L-Arg reduction of the on and off rates for oxygen matches the "impedance" model on ligand binding proposed by us and was well exemplified by cyanide binding to eNOS (*14*). In this case, the effect of L-Arg on k_{-1} is larger than on k_1. However, together with a decrease in k_2, L-Arg drastically enhanced the accumulation of the oxyferrous intermediate. It should be noted that the resolved spectra by global analysis in the absence of L-arginine gave the oxyferrous intermediate a Soret peak at 418 nm for three data sets and 428 nm for one data set. The only time we resolved the 428 nm species was the time we had more rapid scan data in the first 15 ms showing a red shift even though none of these intermediate spectra show a peak greater than 422 nm. When the number of these transiently red shifted spectra was low, the global analysis program had difficulty deconvoluting the optical spectrum of the oxyferrous intermediate.

Stabilization of the oxyferrous intermediate by L-Arg makes physiological sense. When L-Arg binds to the active site, the oxyferrous heme intermediate is stabilized to accept the second electron to accomplish the monooxygenase reaction, while in the absence of L-Arg degradation of oxyferrous heme would form superoxide, a potentially deleterious reactive oxygen species.

3. Existing Mechanistic Complications of the Reaction between NOS and Oxygen.

a. L-Arg Effect and Spectral Variations. The effect of L-Arg on oxygen binding to NOS has been subject to debate. There are several possible reasons for this. The characteristics of the optical spectrum for the oxyferrous NOS intermediate have been controversial. The reported Soret peak position varies from 416 to 430 nm depending on the NOS isozyme species, the temperature, and the presence and absence of L-Arg and BH_4 and their analogues (*18*, *28*−*33*). In the present study, the Soret peak for the putative oxyferrous intermediate shifts from ∼420 nm in the absence of L-Arg to ∼427 nm in the presence of L-Arg. Sato et al. (*28*) also observed similar spectral changes with nNOS. Although Abu-Soud et al. (*18*, *19*) concluded that L-Arg did not affect the optical spectrum or the kinetics of the oxyferrous heme intermediate in either $nNOS_{ox}$ or eNOS, for the latter, parallel spectroscopic data in the presence and absence of L-Arg were not shown, and subtle spectral shifts may have gone unnoticed. A recent study by Marchal et al. demonstrated an effect of L-arginine on $eNOS_{ox}$ reaction with oxygen, with the oxyferrous intermediate showing a shift from 420 to 432 nm (*66*). The observed spectral changes induced by L-arginine are rather similar to our finding in this study. However, the off rate constants were not determined for the reaction without L-arginine, and the on rates were estimated from the data obtained at a single oxygen concentration; thus, a reliable quantitative evaluation of the L-arginine effect was not achieved (*66*).

Another possible cause for the Soret variation of the $Fe^{II}O_2$ intermediate is a variation of the oxygen binding affinity of NOS, which would lead to variable accumulation of the oxyferrous heme intermediate. K_m determination for three NOS isozymes by polarographic methods yielded values of 23.2, 7.7, and 6.3 μM O_2 for nNOS, eNOS, and iNOS, respectively (*67*). The oxygen K_d values calculated from

association and dissociation rate constants ranged from 38 to 122 μM for eNOS and from 59 to 167 μM for $nNOS_{ox}$ (*18*, *19*). The present kinetic measurements with eNOS/$eNOS_{ox}$ gave K_d values between 10 and 45 μM (Table 1). Moreover, the present K_d values obtained in the presence of L-Arg were between 10 and 25 μM (Table 1), even closer to K_m estimations obtained polarographically in the presence of L-Arg (*67*). More reliable K_d values cannot be derived for $eNOS_{ox}$ from the study by Marchal et al. as the off rate constants determined by the *y*-intercept of the secondary plot between observed rates and ligand concentration were found to be less than zero (*66*). This result should not occur theoretically and may be due to an excess of dithionite present in their $eNOS_{ox}$ sample solution, which reduced the effective oxygen concentrations, leading to lower observed rates. We compared our stopped-flow measurements in the presence of L-Arg with those in either air or oxygen-saturated buffer (750 μM after mixing at 4 °C) and found that the oxyferrous complex was fully formed in both cases (data not shown). This indicates that an oxygen level of 150 μM (during reaction with air-saturated buffer) is sufficient to saturate the heme sites in eNOS, and that the K_d for oxygen in the presence of L-Arg must be significantly less than 100 μM, as with a K_d greater than 100 μM it would be impossible to saturate the heme at these oxygen concentrations. Partial saturation of the ferrous heme by oxygen would lead to a blue shift of the Soret peak, which was not observed in this study.

b. How Small is k_{-1}? The k_{-1} value was estimated from the *y*-axis intercept in a secondary plot of the oxygen binding rates (Figure 4). When the *y*-intercept is close to the origin, it is usually necessary to use independent methods to reliably determine the off rate constants. With the current information, it seems likely that the oxygen dissociation rate constant with L-Arg present is below 10 s^{-1}; otherwise the K_d value would be too high. The off rate constants of L-arginine-treated $eNOS_{ox}$ estimated by Marchal et al. are 24 and $\sim$0 s^{-1} in the presence and absence of BH_4 (or other biopterins), respectively (*66*). These numbers are much smaller than previously published (*18*, *19*) and are closer to the numbers obtained in this study, indicating that oxygen dissociation from $Fe^{II}O_2$ is very slow in the presence of L-arginine. On the other hand, the off rate constant estimated for the reactions without L-Arg must be sufficiently large to account for the observed lack of accumulation of oxyferrous intermediate.

c. One or Two Discrete Heme−Oxy Intermediates? Marchal et al. on the basis of their spectral analysis and the reactivity of the oxyferrous heme with CO further proposed that there are two heme−oxy intermediates, $Fe^{II}O_2$ and $Fe^{III}O_2^-$ (or heme−oxy I and heme−oxy II), that exhibit Soret peaks at 420 and 432 nm obtained in the absence and presence of L-Arg, respectively (*66*). This hypothesis provided another interpretation for the observed variation of the Soret peak of the oxyferrous intermediate, but it is yet to be shown whether these "stable" optical species observed at low temperature are pure species. A careful simulation using the measured rates should be able to predict if the spectra recorded at specific time points for the heme−oxy I or II are mixtures of several optical species. Additional methods such as resonance Raman (rR) or FTIR are needed for structural confirmation for this proposal. It is interesting to note that Couture et al. observed a 430 nm heme−oxy II intermediate at 0.6 ms during the reaction between $nNOS_{ox}$ and oxygen even in the absence of L-Arg and BH_4 at 25 °C (*33*), a direct contradiction to the conclusion made by Marchal et al., where a 420 nm species is expected (*66*). rR identified the O−O stretching frequency at 1132 cm^{-1} using $^{16}O_2$ and $^{18}O_2$, which show marginal dependence on L-Arg, L-NHA, or BH_4 (*33*). These observations are at odds with Marchal et al.'s optical assignments and cast serious doubts on the simple optical dissection between $Fe^{II}O_2$ and $Fe^{III}O_2^-$ complexes. For the time being, we have treated $Fe^{II}O_2$ and $Fe^{III}O_2^-$ as two forms in structural resonance that cannot be distinguished optically. Our data analysis supports this assumption. When we used the rate constants obtained by stopped-flow measurements to conduct kinetic simulations, the heme−oxy intermediate never accounted for more than 50% of the total heme in the absence of L-arginine, while in its presence the $Fe^{II}O_2$ (or $Fe^{III}O_2^-$) accumulated to as high as 90% (data not shown), indicating that the heme−oxy I defined by Marchal et al. is probably a mixture of multiple species (*66*). The reason that Couture et al. were able to observe a 430 nm heme−oxy intermediate in the absence of substrate is likely the very short dead time of the instrument and very high oxygen concentration, which allow accumulation of significant amounts of the oxyferrous intermediate (*33*).

d. Heterogeneity of Decay Kinetics. In six out of eight sample combinations, the decay kinetics of $Fe^{II}O_2$ were biphasic (Table 1). Only $eNOS_{ox}$ in the presence of L-Arg showed monophasic decay of the oxyferrous intermediate. The biphasic decay kinetics with similar absorbance contribution observed for full-length eNOS and $eNOS_{ox}$ in the absence of L-Arg are most likely a manifestation of the slight difference between the two heme centers in the dimer. This difference could be due to alterations in porphyrin structure or heme spin state. Protein sample heterogeneity should not be the reason for the biphasic kinetics as the same $eNOS_{ox}$ sample in the presence of L-Arg did not show biphasic kinetics (Table 1). Evidence for structural differences of the two heme centers was present in our previous spectral and kinetic studies of eNOS (*14*, *38*). L-Arg binding also revealed this subtle difference in the heme behavior. This could be simply a consequence of different orientations of the $Fe^{II}O-O$ toward the guanidine of L-Arg in the two monomers, leading to changes in stabilization of the $Fe^{II}O_2$ intermediate by L-Arg.

4. Effect of BH_4 on Oxygen Binding and BH_4 Radical Formation in eNOS and $eNOS_{ox}$. BH_4 was found to have little effect on oxygen binding in both eNOS and $eNOS_{ox}$ regardless of L-Arg binding (Table 1). This is consistent with the considerable distance between the BH_4 binding site and the heme distal coordination site (*20*, *21*). The 10-fold increase in the decay rate constant for oxyferrous $nNOS_{ox}$ upon BH_4 addition contrasts with the observed insensitivity of k_2 to BH_4 in eNOS/$eNOS_{ox}$ (Table 1). At 4 °C, the decay rate constant for $Fe^{II}O_2$ in $eNOS_{ox}$ was 1.4 s^{-1} in the presence of L-Arg and BH_4. At 24 °C and high $eNOS_{ox}$ concentration, the decay rate was increased to about 10 s^{-1} and paralleled formation of the BH_4 radical and ferric heme (Figure 6A). Although this situation is similar to that reported for $iNOS_{ox}$ (*34*, *35*), the present RFQ EPR kinetic measurements are the first to establish that eNOS has a similar mechanism,

with BH_4 donating the second electron to oxyferrous heme in the monooxygenase reaction. In the presence of L-Arg and BH_4, only one radical species was observed during the whole reaction between ferrous heme and oxygen (Figure 5). These data support the following reaction scheme:

$$\text{L-Arg}-\text{Fe(II)}-BH_5^{+} + O_2 \underset{k_{-1}}{\overset{k_1}{\leftrightarrow}} \text{L-Arg}-\text{Fe}^{\text{II}}O_2-BH_5^{+} \xrightarrow[+H^+]{k_2} \text{Fe(III)}-BH_4^{+}* + \text{L-NHA} + H_2O \quad (5)$$

In the absence of L-Arg, the following reactions likely happen:

$$\text{Fe(II)}-BH_5^{+} + O_2 \underset{k_{-1}}{\overset{k_1}{\leftrightarrow}} \text{Fe}^{\text{II}}O_2-BH_5^{+} \xrightarrow[+H^+]{k_2} \text{Fe(III)}-BH_4^{+}* + H_2O_2 \quad (6)$$

Comparing eq 4 with eq 6, it is plausible to propose that one function of BH_4 is to replace superoxide formation by hydrogen peroxide formation in the absence of substrate, similar to the reactons observed for nNOS (*68*). H_2O_2 is not easily converted to peroxynitrite in the presence of NO, reducing the cytotoxicity of the nonproductive reaction. This may be more important for self-inhibition of nNOS by NO than for eNOS as this isozyme forms less NO (*5*). A separate study using rapid-scan and rapid-freeze-quench EPR kinetic measurements has been published recently that investigates in detail the effects of substrate and BH_4 on three different oxygen-induced radical intermediates of $eNOS_{ox}$ (*69*). Transition from a peroxyl radical to a BH_4 radical in the absence of substrate was observed and seemed to support the mechanism in eq 6.

In conclusion, a novel chemical quench/HPLC analytic method permitted simultaneous quantitation of all three redox species of biopterin. This method was used to demonstrate that inactivation of eNOS correlates with BH_4 autoxidation and that this inactivation was reversible. In contrast to earlier publications, L-Arg had a substantial effect on the interaction of oxygen with ferrous eNOS, leading to a sizable decrease in the oxygen binding rate constants and the decay rate of the oxyferrous intermediate. Although BH_4 had no apparent effect on the oxygen binding kinetics, the three-way kinetic correlation among heme EPR, heme optical, and radical EPR signals demonstrated that BH_4 provides the second reducing equivalent for monooxygenation of L-Arg in eNOS.

ACKNOWLEDGMENT

We thank Dr. Gang Wu for his assistance in conducting the rapid-freeze-quench EPR experiments. We also thank Dr. Lee-Ho Wang for his guidance in developing the eNOS yeast expression system and Dr. Richard J. Kulmacz for his reading and fruitful discussion of the manuscript.

REFERENCES

1. Feldman, P. L., Griffith, O. W., and Stuehr, D. J. (1993) The surprising life of NO, *Chem. Eng. News 51*, 26−38.
2. Raman, C. S., Martásek, P., and Masters, B. S. S. (2000) Structure themes determining function in nitric oxide synthase, in *The Phorphyrin Handbook* (Kadish, K. M., Smith, K. M., and Guilard, R., Eds.) pp 293−339, Academic Press, New York.
3. Roman, L. J., Martásek, P., and Masters, B. S. S. (2002) Intrinsic and extrinsic modulation of nitric oxide synthase activity, *Chem. Rev. 102*, 1179−1189.
4. Stuehr, D. J. (1999) Mammalian nitric oxide synthases, *Biochim. Biophys. Acta 1411*, 217−230.
5. Wei, C.-C., Crane, B. R., and Stuehr, D. J. (2003) Tetrahydrobiopterin radical enzymology, *Chem. Rev. 103*, 2365−2383.
6. Tayeh, M. A., and Marletta, M. A. (1989) Macrophage oxidation of L-arginine to nitric oxide, nitrite, and nitrate. Tetrahydrobiopterin is required as a cofactor, *J. Biol. Chem. 264*, 19654−19658.
7. Kwon, N. S., Nathan, C. F., and Stuehr, D. J. (1989) Reduced biopterin as a cofactor in the generation of nitrogen oxides by murine macrophages, *J. Biol. Chem. 264*, 20496−20501.
8. Hevel, J. M., and Marletta, M. A. (1992) Macrophage nitric oxide synthase: relationship between enzyme-bound tetrahydrobiopterin and synthase activity, *Biochemistry 31*, 7160−7165.
9. Rusche, K. M., and Marletta, M. A. (2001) Reconstitution of pterin-free inducible nitric-oxide synthase, *J. Biol. Chem. 276*, 421−427.
10. Kirsch, M., Korth, H. G., Stenert, V., Sustmann, R., and de Groot, H. (2003) The autoxidation of tetrahydrobiopterin revisited. Proof of superoxide formation from reaction of tetrahydrobiopterin with molecular oxygen, *J. Biol. Chem. 278*, 24481−24490.
11. Blair, J. A., and Pearson, A. J. (1974) Kinetics and mechanism of the autoxidation of the 2-amino-4-hydroxy-5,6,7,8-tetrahydropteridines, *J. Chem. Soc., Perkin Trans. 2* 80−88.
12. Komori, Y., Hyun J., Chiang, K., and Fukuto, J. M. (1995) The role of thiols in the apparent activation of rat brain nitric oxide synthase (NOS), *J. Biochem. 117*, 923−927.
13. Hofmann, H., and Schmidt, H. H. H. W. (1995) Thiol dependence of nitric oxide synthase, *Biochemistry 34*, 13443−13452.
14. Berka, V., and Tsai, A.-L. (2000) Characterization of interactions among the heme center, tetrahydro-biopterin and l-arginine binding sites of ferric eNOS using imidazole, cyanide and nitric oxide as probes, *Biochemistry 39*, 9373−9383.
15. Presta, A., Siddhanta, U., Wu, C., Sennequier, N., Huang, L., Abu-Soud, H. M., Erzurum, S., and Stuehr, D. J. (1998) Comparative functioning of dihydro- and tetrahydropterins in supporting electron transfer, catalysis, and subunit dimerization in inducible nitric oxide synthase, *Biochemistry 37*, 298−310.
16. Groves, J. T., and Wang, C. C. (2000) Nitric oxide synthase: models and mechanisms, *Curr. Opin. Chem. Biol. 4*, 687−695.
17. Hurshman, A. R., and Marletta, M. A. (2002) Reactions catalyzed by the heme domain of inducible nitric oxide synthase: evidence for the involvement of tetrahydrobiopterin in electron transfer, *Biochemistry 41*, 3439−3456.
18. Abu-Soud, H. M., Gachhui, R., Raushel, F. M., and Stuehr, D. J. (1997) The ferrous-dioxy complex of neuronal nitric oxide synthase. Divergent effects of L-arginine and tetrahydrobiopterin on its stability, *J. Biol. Chem. 272*, 17349−17353.
19. Abu-Soud, H. M., Ichimori, K., Presta, A., and Stuehr, D. J. (2000) Electron transfer, oxygen binding, and nitric oxide feedback inhibition in endothelial nitric-oxide synthase, *J. Biol. Chem. 275*, 17349−17357.
20. Raman, C. S., Li, H., Martásek, P., Král, V., Masters, B. S. S., and Poulos, T. L. (1998) Crystal structure of constitutive endothelial nitric oxide synthase: a paradigm for pterin function involving a novel metal center, *Cell 95*, 1−20.
21. Fischmann, T. O., Hruza, A., Xiao, D. N., Fossetta, J. D., Lunn, C. A., Dolphin, E., Prongay, A. J., Reichert, P., Lundell, D. J., Narula, S. K., and Weber, P. C. (1999) Structural characterization of nitric oxide synthase isoforms reveals striking active-site conservation, *Nat. Struct. Biol. 6*, 233−242.
22. Stevenson, T. H., Gutierrez, A. F., Alderton, W. K., Lian, L., and Scrutton, N. S. (2001) Kinetics of CO binding to the haem domain of murine inducible nitric oxide synthase: differential effects of haem domain ligands, *Biochem. J. 358*, 201−208.
23. Sato, H., Nomura, S., Sagami, I., Ito, O., Daff, S., and Shimizu, T. (1998) CO binding studies of nitric oxide synthase: effects of the substrate, inhibitors and tetrahydrobiopterin, *FEBS Lett. 430*, 377−380.
24. Abu-Soud, H. M., Wu, C., Ghosh, D. K., and Stuehr, D. J. (1998) Stopped-flow analysis of CO and NO binding to inducible nitric oxide synthase, *Biochemistry 37*, 3777−3786.
25. Scheele, J. S., Bruner, E., Kharitonov, V. G., Martásek, P., Roman, L. J., Masters, B. S., Sharma, V. S., and Magde, D. (1999) Kinetics of NO ligation with nitric-oxide synthase by flash photolysis and stopped-flow spectrophotometry, *J. Biol. Chem. 274*, 13105−13110.

26. Négrerie, M., Berka, V., Vos, M. H., Liebl, U., Lambry, J.-C., Tsai, A.-L., and Martin, J.-L. (1999) Geminate recombination of nitric oxide to endothelial NO-synthase and mechanistic implications, *J. Biol. Chem. 274*, 24694−702.
27. Migita, C. T., Salerno, J. C., Masters, B. S., Martásek, P., McMillan, K., and Ikeda-Saito, M. (1997) Substrate binding-induced changes in the EPR spectra of the ferrous nitric oxide complexes of neuronal nitric oxide synthase, *Biochemistry 36*, 10987−10992.
28. Sato, H., Sagami, I., Daff, S., and Shimizu, T. (1998) Autoxidation rates of neuronal nitric oxide synthase: effects of the substrates, inhibitors, and modulators, *Biochem. Biophys. Res. Commun. 253*, 845−849.
29. Bec, N., Gorren, A. C., Voelker, C., Mayer, B., and Lange, R. (1998) Reaction of neuronal nitric-oxide synthase with oxygen at low temperature. Evidence for reductive activation of the oxy-ferrous complex by tetrahydrobiopterin, *J. Biol. Chem. 273*, 13502−13508.
30. Ledbetter, A. P., McMillan, K., Roman, L. J., Masters, B. S., Dawson, J. H., and Sono, M. (1999) Low-temperature stabilization and spectroscopic characterization of the dioxygen complex of the ferrous neuronal nitric oxide synthase oxygenase domain, *Biochemistry 38*, 8014−8021.
31. Boggs, S., Huang, L., and Stuehr, D. J. (2000) Formation and reactions of the heme-dioxygen intermediate in the first and second steps of nitric oxide synthesis as studied by stopped-flow spectroscopy under single-turnover conditions, *Biochemistry 39*, 2332−2339.
32. Gorren, A. C., Bec, N., Schrammel, A., Werner, E. R., Lange, R., and Mayer, B. (2000) Low-temperature optical absorption spectra suggest a redox role for tetrahydrobiopterin in both steps of nitric oxide synthase catalysis, *Biochemistry 39*, 11763−11770.
33. Couture, M., Stuehr, D. J., and Rousseau, D. L. (2000) The ferrous dioxygen complex of the oxygenase domain of neuronal nitric-oxide synthase, *J. Biol. Chem. 275*, 3201−3205.
34. Hurshman, A. R., Krebs, C., Edmondson, D. E., Huynh, B. H., and Marletta, M. A. (1999) Formation of a pterin radical in the reaction of the heme domain of inducible nitric oxide synthase with oxygen, *Biochemistry 38*, 15689−15696.
35. Wei, C. C., Wang, Z. Q., Wang, Q., Meade, A. L., Hemann, C., Hille, R., and Stuehr, D. J. (2001) Rapid kinetic studies link tetrahydrobiopterin radical formation to heme-dioxy reduction and arginine hydroxylation in inducible nitric-oxide synthase, *J. Biol. Chem. 276*, 315−319.
36. Schmidt, P. P., Lange, R., Gorren, A. C., Werner, E. R., and Mayer, B, Andersson KK. (2001) Formation of a protonated trihydrobiopterin radical cation in the first reaction cycle of neuronal and endothelial nitric oxide synthase detected by electron paramagnetic resonance spectroscopy, *J. Biol. Inorg. Chem. 6*, 151−158.
37. Bec, N., Gorren, A. F. C., Mayer, B., Schmidt, P. P., Andersson, K. K., and Lange, R. (2000) The role of tetrahydrobiopterin in the activation of oxygen by nitric-oxide synthase, *J. Inorg. Biochem. 81*, 207−211.
38. Du, M., Yeh, H. C., Berka, V., Wang, L. H.,and Tsai, A.-L. (2003) Redox properties of human endothelial nitric oxide synthase oxygenase and reductase domains purified from yeast expression system, *J. Biol. Chem. 278*, 6002−6011.
39. Wei, C. C., Wang, Z. Q., Hemann, C., Hille, R., Stuehr, D. J. (2003) A tetrahydrobiopterin radical forms and then becomes reduced during Nomega-hydroxyarginine oxidation by nitric-oxide synthase, *J. Biol. Chem. 278*, 46668−46673.
40. Chen, P.-F., Tsai, A.-L. Berka, V., and Wu, K. K. (1996) Endothelial nitric oxide synthase: evidence for bidomain structure and successful reconstitution of catalytic activity from two separate domains generated by a baculovirus expression system, *J. Biol. Chem. 271*, 14631−14635.
41. Martásek, P., Liu, Q., Liu, J., Roman, L. J., Gross, S. S., Sessa, W. C., and Masters, B. S. S. (1996) Characterization of bovine endothelial nitric oxide synthase expressed in E. coli, *Biochem. Biophys. Res. Commun. 219*, 359−365.
42. Feelisch, M., and Noack, E. A. (1987) Nitric oxide (NO) formation from nitrovasodilators occurs independently of hemoglobin or non-heme iron, *Eur. J. Pharmacol. 139*, 19−30.
43. Chen, P.-F., Tsai, A.-L., and Wu, K. K. (1995) Cysteine 99 of endothelial nitric oxide synthase (NOS-III) is critical for tetrahydrobiopterin-dependent NOS-III stability and activity, *Biochem. Biophys. Res. Commun. 215*, 1119−1129.
44. Hales, B. J. (1993) Intrinsic and extrinsic paramagnets as probes of metal clusters, *Methods Enzymol. 227*, 384−395.
45. Davis, M. D., Kaufman, S., and Milstien, S. (1988) The auto-oxidation of tetrahydrobiopterin, *Eur. J. Biochem. 173*, 345−351.
46. Tani, Y., and Ohno, T. (1993) Analysis of 6R- and 6S-tetrahydrobiopterin and other pterins by reversed-phase ion-pair liquid-chromatography with fluorimetric detection by post-column sodium nitrite oxidation, *J. Chromatogr., B 617*, 249−255.
47. Brautigam, M., and Dreesen, R. (1982) Determination of L-erythro-tetrahydrobiopterin in biological tissues by high-pressure liquid chromatography and electrochemical detection, *Hoppe-Seyler's Z. Physiol. Chem. 363* (Suppl.), 1203−1207.
48. Howells, D. W., Smith, I., and Hyland, K. (1986) Estimation of tetrahydrobiopterin and other pterins in cerebrospinal fluid using reversed-phase high-performance liquid chromatography with electrochemical and fluorescence detection, *J. Chromatogr. 381*, 285−94.
49. Baek, K. J., Thiel, B. A., Lucas, S., and Stuehr, D. J. (1993) Macrophage nitric oxide synthase subunits. Purification, characterization, and role of prosthetic groups and substrate in regulating their association into a dimeric enzyme, *J. Biol. Chem. 268*, 21120−21129.
50. Tzeng, E., Billiar, T. R., Robbins, P. D., Loftus, M., and Stuehr, D. J. (1995) Expression of human inducible nitric oxide synthase in a tetrahydrobiopterin (H4B)-deficient cell line: H4B promotes assembly of enzyme subunits into an active dimer, *Proc. Natl. Acad. Sci. U.S.A. 92*, 11771−11775.
51. Klatt, P., Pfeiffer, S., List, B. M., Lehner, D., Glatter, O., Bächinger, H. P., Werner, E. R., Schmidt, K., and Mayer, B. (1996) Characterization of heme-deficient neuronal nitric-oxide synthase reveals a role for heme in subunit dimerization and binding of the amino acid substrate and tetrahydrobiopterin, *J. Biol. Chem. 271*, 7336−7342.
52. Gorren, A. C. F., List, B. M., Schrammel, A., Pitters, E., Hemmens, B., Werner, E. R., Schmidt, K. and Mayer, B. (1996) Tetrahydrobiopterin-free neuronal nitric oxide synthase: evidence for two identical highly anticooperative pteridine binding sites, *Biochemistry 35*, 16735−16745.
53. List, B. M., Klösch, B., Völker, C., Gorren, A. C. F., Sessa, W. C., Werner, E. R., Kukovetz, W. R., Schmidt, K., and Mayer, B. (1997) Characterization of bovine endothelial nitric oxide synthase as a homodimer with down-regulated uncoupled NADPH oxidase activity: tetrahydrobiopterin binding kinetics and role of haem in dimerization, *Biochem. J. 323*, 159−165.
54. Bird, L. E., Ren. J., Zhang, J., Foxwell, N., Hawkins, A. R., Charles, I. G., and Stammers, D. K. (2002) Crystal structure of SANOS, a bacterial nitric oxide synthase oxygenase protein from Staphylococcus aureus *Structure 10*, 1687−1696.
55. Pant, K., Bilwes, A. M., Adak, S., Stuehr, D. J., and Crane, B. R. (2002) Structure of a nitric oxide synthase heme protein from Bacillus subtilis, *Biochemistry 41*, 11071−11079.
56. Klatt, P., Schmidt, M., Leopold, E., Schmidt, K., Werner, E. R., and Mayer, B. (1994) The pteridine binding site of brain nitric oxide synthase, *J. Biol. Chem. 269*, 13861−13866.
57. Schmidt, H. H. H. W., Smith, R. W., Nakane, M., and Murad, F. (1992) Ca^{2+}/calmodulin-dependent NO synthase type I: a biopter-oflavoprotein with Ca^{2+}/calmodulin-independent diaphorase and reductase activities, *Biochemistry 31*, 3243−3249.
58. Mayer, B., John, M., Heinzel, B., Werner, E. R., Wachter, H., Schultz, G. and Böhme, E. (1991) Brain nitric oxide synthase is a biopterin- and flavin-containing multi-functional oxido-reductase, *FEBS Lett. 288*, 187−191.
59. Fukushima, T., Nixon, J. C. (1980) Analysis of reduced forms of biopterin in biological tissues and fluids, *Anal. Biochem. 102*, 176−188.
60. Stuehr, D. J., Kwon, N. S., and Nathan, C. F. (1990) FAD and GSH participate in macrophage synthesis of nitric oxide, *Biochem. Biophys. Res. Commun. 168*, 558−565.
61. Sono, M., Ledbetter, A. P., McMillan, K., Roman, L. J., Shea, T. M., Masters, B. S. S., and Dawson, J. H. (1999) Essential thiol requirement to restore pterin- or substrate-binding capability and to regenerate native enzyme-type high-spin heme spectra in the Escherichia coli-expressed tetrahydrobiopterin-free oxygenase domain of neuronal nitric oxide synthase, *Biochemistry 38*, 15853−15862.
62. Gorren, A. C. F., Schrammel, A., Schmidt, K., and Mayer, B. (1997) Thiols and neuronal nitric oxide synthase: complex formation, competitive inhibition, and enzyme stabilization, *Biochemistry 36*, 4360−4366.

63. Vasquez-Vivar, J., Whitsett, J., Martásek, P., Hogg, N., and Kalyanaraman, B. (2001) Reaction of tetrahydrobiopterin with superoxide: EPR-kinetic analysis and characterization of the pteridine radical, *Free Radical Biol. Med. 31*, 975−985.
64. Ghosh, S., Wolan, D., Adak, S., Crane, B. R., Kwon, N. S., Tainer, J. A., Getzoff, E. D., and Stuehr, D. J. (1999) Mutational analysis of the tetrahydrobiopterin-binding site in inducible nitric-oxide synthase, *J. Biol. Chem. 274*, 24100−24112.
65. Mayer, B., Wu, C., Gorren, A. C., Pfeiffer, S., Schmidt, K., Clark, P., Stuehr, D. J., Werner, E. R. (1997) Tetrahydrobiopterin binding to macrophage inducible nitric oxide synthase: heme spin shift and dimer stabilization by the potent pterin antagonist 4-amino-tetrahydrobiopterin, *Biochemistry 36*, 8422−8427.
66. Marchal, S., Gorren, A. C., Sorlie, M., Andersson, K. K., Mayer, B., and Lange, R. (2004) Evidence of two distinct oxygen complexes of reduced endothelial nitric oxide synthase, *J. Biol. Chem. 279*, 19824−19831.
67. Rengasamy, A, and Johns, R. A. (1996) Determination of Km for oxygen of nitric oxide synthase isoforms, *J. Pharmacol. Exp. Ther. 276*, 30−33.
68. Rosen, G. M., Tsai, P., Weaver, J., Porasuphatana, S., Roman, L. J., Starkov, A. A., Fiskum, G., and Pou, S. (2002) The role of tetrahydrobiopterin in the regulation of neuronal nitric-oxide synthase-generated superoxide, *J. Biol. Chem. 277*, 40275−40280.
69. Berka, V., Wu, G., Yeh, H. C., Palmer, G., and Tsai, A.-L. (2004) Three different oxygen-induced radical species in eNOS oxygenase under regulation by L-arginine and tetrahydrobiopterin, *J. Biol. Chem. 279*, 32234−32251.

BI049026J